

1 **Solar Energetic Electron Access to the Moon within**
2 **the Terrestrial Magnetotail and Shadowing by the**
3 **Lunar Surface**

4 **Lucas Liuzzo¹, Andrew R. Poppe¹, Christina O. Lee¹, and Vassilis**
5 **Angelopoulos²**

6 ¹Space Sciences Laboratory, University of California, Berkeley, CA, USA

7 ²Department of Earth, Planetary, and Space Sciences, University of California, Los Angeles, CA, USA

8 **Key Points:**

- 9 • High-energy solar energetic electrons (SEEs) have direct access to the lunar en-
10 vironment when in the terrestrial magnetotail
11 • Precipitation onto the lunar nightside carves-out electrons from the ambient dis-
12 tribution, generating extended shadows far from the Moon
13 • When in the tail, the lunar surface is non-uniformly bombarded by Earthward-
14 traveling SEEs, with reduced access to the dayside hemisphere

15 Abstract

16 We present measurements of 30–700 keV Solar Energetic Electrons (SEEs) near the Moon
17 when within the terrestrial magnetotail by the *Acceleration, Reconnection, Turbulence,*
18 *and Electrodynamics of the Moon’s Interaction with the Sun* spacecraft. Despite their
19 detection deep within the tail, the incident flux and spectral shape of these electrons are
20 nearly identical to measurements taken upstream of Earth in the solar wind by the Wind
21 spacecraft; however, their pitch angle distribution is isotropized compared to the more
22 field-aligned distribution upstream. We illustrate that SEEs initially traveling Earthward
23 precipitate onto the lunar far-side, generating extended shadows in the cis-lunar elec-
24 tron distribution. By modeling the dynamics of these electrons, we show that their pre-
25 cipitation patterns on the lunar near-side are comparatively reduced. The non-uniform
26 precipitation and accessibility of potentially hazardous electrons to the Moon’s surface
27 are highly relevant in the context of astronaut safety during the planned exploration of
28 the lunar environment.

29 Plain Language Summary

30 The Moon is located within the tail of Earth’s magnetosphere during one-third of
31 its orbit. Although the strong terrestrial magnetic field prevents high-energy particles
32 from reaching Earth’s surface, the Moon does not receive the same protection when it
33 is within the terrestrial magnetotail. Instead, we show that the high-energy electron flux
34 near the Moon is unchanged during intense solar energetic electron events compared to
35 measurements taken far upstream of Earth. However, the precipitation of these parti-
36 cles onto the lunar surface is non-uniform. Since these electrons gain access to the mag-
37 netosphere from down-tail of the Moon, they preferentially bombard the lunar far-side
38 surface. This creates a shadow in the electrons on the nearside that extends far beyond
39 the Moon toward Earth. Hence, despite the high flux of these particles that are poten-
40 tially hazardous to future activities on the lunar surface, there exist regions across the
41 lunar near-side where the relative flux of these electrons is reduced relative to the up-
42 stream value when the Moon is within the magnetotail. These findings provide context
43 for the fundamental scientific understanding of high-energy solar electrons and their ac-
44 cess to the lunar surface.

45 **1 Introduction**

46 During the Moon's (radius $R_L = 1,737.4$ km) 29.5 d synodic period as it orbits
 47 Earth, it passes through the terrestrial magnetotail for ~ 1 week. Here, the lunar en-
 48 vironment is ostensibly shielded from the low-energy solar wind plasma and is instead
 49 exposed to the tenuous plasma comprising the tail (e.g., Liuzzo, Poppe, & Halekas, 2022;
 50 Terada et al., 2017) nearly $\sim 60R_E$ from Earth (radius $R_E = 6,378$ km). However,
 51 besides the solar wind, the Sun is also a source of high-energy ions and electrons that
 52 are associated with flares and coronal mass ejections (CMEs). Recently, Liuzzo et al. (2023)
 53 found that solar energetic protons have nearly unrestricted access to the Moon while em-
 54 bedded within the terrestrial magnetotail. However, there are few studies investigating
 55 solar energetic electron (SEE) access to the lunar environment within the tail. Recently,
 56 Jordan et al. (2023) estimated that incident electrons at energies below 100s of MeV would
 57 be deflected by the tail since their gyroradii are small on the scales of the magnetotail.
 58 Hence, they suggest that the Moon may not be exposed to any SEEs during each mag-
 59 netotail transit. This contradicts observations from Explorer 35 spacecraft which detected
 60 SEEs within the magnetotail at energies as low as ~ 50 keV (e.g., Lin, 1968; Van Allen
 61 & Ness, 1969).

62 Therefore, understanding and quantifying the accessibility of high-energy electrons
 63 to the Moon's surface within the magnetotail is imperative for characterizing the lunar
 64 environment. In addition, constraining the resulting surface fluxes is critical when in-
 65 vestigating potential hazards to astronauts during future missions to the Moon. We present
 66 a case study of two SEE events where the Moon was bombarded by a population of high-
 67 energy electrons when located within the tail. By comparing observations within the tail
 68 to concurrent measurements taken upstream of Earth, we find that the tail is a poor shield
 69 to the incident electrons, resulting in little-to-no change to the local fluxes. However, their
 70 pitch angle distributions are altered from highly field-aligned upstream of Earth to isotropic
 71 at most locations within the tail. We identify regions in cis-lunar space where particles
 72 precipitate onto the lunar nightside and are carved out of the velocity distribution. This
 73 generates an extended shadow that partially shields the Moon's dayside surface from SEEs
 74 that would have otherwise mirrored near Earth and returned to the Moon, resulting in
 75 a lower electron flux on the dayside compared to the nightside. A similar process occurs
 76 in the solar wind, but the comparatively stable orientation of the magnetotail lobe field,

77 along with the initial arrival of SEEs from down-tail, portends a more predictable cis-
 78 lunar shadow of reduced fluxes near the dayside close to the Earth-Moon line.

79 **2 Methods**

80 Since 2004, the Wind spacecraft (Harten & Clark, 1995) has been located $\sim 200R_E$
 81 upstream of Earth, providing continuous monitoring of the incoming plasma and ener-
 82 getic particle environment. The spacecraft's Three-Dimensional Plasma instrument (3DP;
 83 Lin et al., 1995) measures particles over a large range of energies, using an Electrostatic
 84 Analyser (ESA) that detects electrons at energies from $\sim 5 \text{ eV} \leq E \leq 30 \text{ keV}$ and a
 85 Solid State Telescope (SST) that observes electrons from $20 \text{ keV} \leq E \leq 1 \text{ MeV}$. The
 86 two probes (P1 and P2) of the THEMIS-ARTEMIS mission (*Time History of Events and*
 87 *Macroscale Interactions during Substorms-Acceleration, Reconnection, Turbulence, and*
 88 *Electrodynamics of the Moon's Interaction with the Sun*; hereafter, ARTEMIS), which
 89 have been orbiting the Moon since 2011, have identical instrumentation including an elec-
 90 tron ESA ($5 \text{ eV} \leq E \leq 30 \text{ keV}$) and SST ($25 \text{ keV} \leq E \leq 1\text{MeV}$) that share heritage
 91 with 3DP on Wind (see Angelopoulos, 2011; McFadden et al., 2008). The similarities
 92 between the instruments, the large spatial separation between the spacecraft, and the
 93 Moon's (and ARTEMIS probes') monthly transit through the magnetotail provide a unique
 94 opportunity to constrain how Earth's magnetosphere shapes the properties of incident
 95 electrons during SEE events and investigate the degree to which they are prevented from
 96 reaching the lunar surface.

97 To account for slight differences between the instrument calibrations and responses,
 98 we first investigate an SEE event that was observed by the three spacecraft when located
 99 within the solar wind. On 15 December 2023, SEE measurements from the Wind elec-
 100 tron ESA and SST were a factor of 3 and 2 lower, respectively, than the ARTEMIS ob-
 101 servations (for further detail, see Figure S1 in the Supporting Information). To ensure
 102 the measurements have a similar baseline for comparison, we multiply the Wind obser-
 103 vations by these calibration factors, allowing for more accuracy when quantifying the role
 104 that Earth's tail has on these electrons.

105 **3 Results**

106 **3.1 SEE observations within the tail**

107 At 03:26 UTC on 01 September 2023, an M1.2 solar flare erupted from active re-
 108 gion AR13413, generating a burst of solar energetic electrons. Figure 1 displays obser-
 109 vations from Wind and ARTEMIS P2 during this event, with electron pitch angle dis-
 110 tributions (PADs) included at select energies. The P2 ESA PAD (14 keV) has been sam-
 111 pled to a 30s resolution to match the SST sampling rate more closely and improve signal-
 112 to-noise. To facilitate comparison, the PADs are normalized by the maximum detected
 113 flux at each time. Panel 1e provides the magnetic field in Geocentric Solar Ecliptic (GSE)
 114 coordinates, where x points from Earth toward the Sun, y lies within the ecliptic plane
 115 (opposite Earth's orbital motion), and z is normal to the ecliptic. P1 had a low sampling
 116 resolution during this time, so its observations are not included.

117 Figure 1 illustrates that electrons from the 01 September 2023 SEE event first ar-
 118 rived to Wind and P2 approximately 20 min after the flare, with a clear dispersive sig-
 119 nture in the differential flux. The similarity between the spectra observed by the space-
 120 craft (panel 1f) provides confidence that these electrons originated from the same source,
 121 but the omnidirectional fluxes observed by ARTEMIS are up to a factor of 1.5 higher
 122 than those observed by Wind, with the largest differences occurring for energies $E \lesssim$
 123 30 keV. Despite the similarities between the two-hour-averaged spectra, panels 1c and
 124 1d highlight differences between the electron PADs. The distribution of the SEEs ob-
 125 served by Wind were nearly field-aligned: the pitch angles of 310 keV electrons were max-
 126 imized near $\alpha \lesssim 45^\circ$ while 13 keV electrons remained below $\alpha \lesssim 10^\circ$. The field-aligned
 127 nature of these electrons for nearly eight hours after their initial onset indicates their con-
 128 tinual streaming outward from the Sun past the Wind spacecraft. As in panel 1a, the
 129 dispersive signature of these SEEs is visible in the electron PADs. However, the electron
 130 PADs observed by ARTEMIS were not field aligned: panel 1d instead illustrates that
 131 they were isotropic across multiple energies. The magnetic field within the tail was mainly
 132 pointed toward Earth ($B_x > 0$), so electrons originating from down-tail with pitch an-
 133 gles $0^\circ \leq \alpha \leq 90^\circ$ traveled Earthward as they passed the ARTEMIS probes. On the
 134 other hand, electrons with pitch angles of $90^\circ \leq \alpha \leq 180^\circ$ must have traveled *tailward*
 135 as they passed the probes. These distributions suggest that SEEs with anti-field-aligned
 136 pitch angles initially passed the Moon from down-tail and mirrored in the enhanced near-

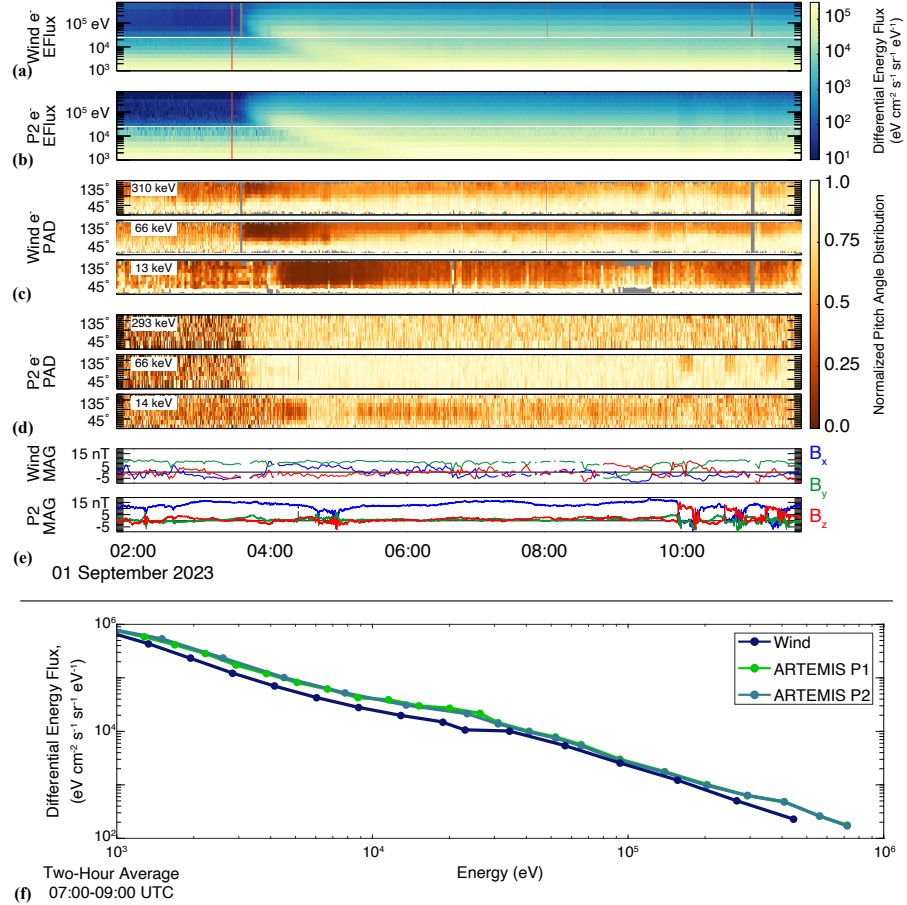


Figure 1. SEE observations on 01 September 2023. Panels (a) and (b) display Wind and P2 differential energy fluxes, (c) and (d) show the PADs normalized to the maximum value at each point in time, and (e) displays the magnetic field in GSE. Gray shading in (a) and (c) denotes periods without Wind data. Panel (f) shows a two-hour average (from 07:00–09:00 UTC) of the differential energy fluxes. The vertical red lines in (a–b) denote the time of the M1.2 flare.

137 Earth field before returning to the lunar environment and being detected a second time.
 138 This is consistent with the fluxes observed by ARTEMIS being enhanced by ~ 1.5 times
 139 compared to Wind. This factor being slightly less than two suggests that some of the
 140 initially Earthward-traveling electrons were scattered or lost before returning to the Moon.

141 Such a mechanism is further supported by the observations near 10:00 UTC. Here,
 142 P2 was located between the Earth and Moon approximately $10R_L$ above the surface and
 143 observed three brief reductions in the differential energy flux, each lasting ~ 20 min (see
 144 Figures 1b and 1d). During these observations, the magnetic field rotated to be nearly

aligned with the $+z$ -direction (panel 1e), indicating that P2 was connected to a magnetosheath field line; inspection of the ESA ion fluxes during this time (not shown) also confirms the presence of magnetosheath plasma. Since the probe was no longer on a field line connected to Earth, the mirrored component of the electron flux disappeared resulting in a drop-out of electrons at pitch angles $\alpha \geq 90^\circ$ (panel 1d).

To further investigate this effect, Figure 2 shows electron energy fluxes (2a–b), PADs (2c–d), and magnetic field (2e) detected by ARTEMIS during a separate SEE event on 31 July 2023 (generated by an M4.1 flare and a CME that occurred three days earlier). Observations from Wind during this time are not included, but similar to the 01 September 2023 event, the SEEs were highly field-aligned far upstream of Earth. Even while deep within the magnetotail, the probes detected enhanced SEE fluxes as shown in Figure 2. Note that the PADs in panels 2c and 2d are not normalized, and that the 1–10 keV PADs (detected by the ESAs) have been sampled to match the temporal resolutions of the SSTs (~ 30 s).

As with the September event (see Figure 1), the electron PADs detected by ARTEMIS during this July event were mainly isotropic across a wide range of energies from $1 \text{ keV} \leq E \leq 300 \text{ keV}$ (see panels 2c and 2d). However, both probes passed through regions where the electron fluxes dropped, with distinct bite-outs in the observed PADs. Near closest approach, P1 detected one such feature (magenta horizontal bar in Figure 2), where the electron fluxes were reduced in ESA energy channels by a factor of ~ 2 . Since the attenuators on the ARTEMIS SSTs were activated near closest approach, there are no usable SST measurements from P1 after 18:10 UTC (gray regions in panel 2c). However, the pitch angle distribution measured by ESA indicates that electrons near 18:30 UTC were initially field-aligned (i.e., depletions at pitch angles $90^\circ < \alpha \leq 180^\circ$ were detected), before transitioning to reductions at all pitch angles near 18:45 UTC, followed by a population of anti-field-aligned electrons at 19:20 UTC and 19:30 UTC.

Similarly, P2 detected seven such depletions in the electron fluxes (magenta bars in Figure 2). As seen in panel 2d, these flux depletions were associated with variable dropouts in the PADs, at times occurring across all pitch angles while at others occurring only for field-aligned ($0^\circ \leq \alpha < 90^\circ$) electrons. For example near 15:10 UTC, the 1–10 keV electron distribution measured by the ESA on P2 was first reduced at pitch angles $0^\circ \leq \alpha < 90^\circ$, before displaying a full reduction across all pitch angles after 15:30 UTC. Five

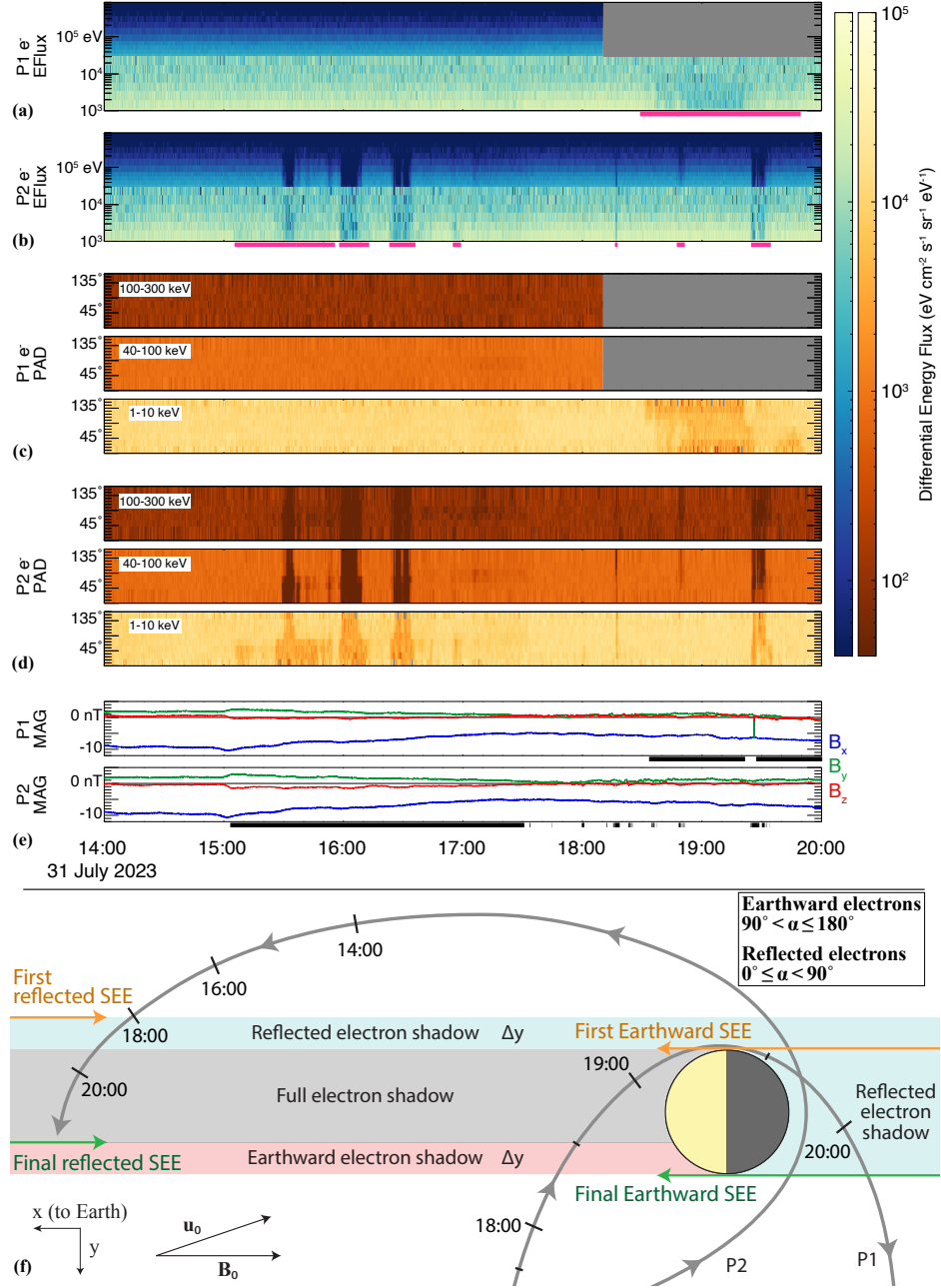


Figure 2. ARTEMIS SEE observations on 31 July 2023 within Earth's southern magnetotail lobe. Black bars along the bottom of (e) show times where the probes were magnetically connected to the lunar surface, while magenta bars in (a) and (b) indicate regions depleted of SEEs. The P1 data gap at high energies corresponds to closest approach, where the SST attenuator was activated. Panel (f) displays a schematic explaining the SEE drop-outs, projected onto the GSE x - y plane and viewed from above the Moon's North pole. Colored regions correspond to SEE shadows, for (blue) reflected electrons, (red) Earthward electrons, and (gray) all electrons, and Δy indicates the electron's displacement in the $-y$ -direction caused by magnetotail convection.

177 minutes later, the flux of only field-aligned electrons was again reduced until approxi-
 178 mately 16:00 UTC. Similar features (but less extended in time) were detected in the pitch
 179 angles of higher-energy electrons as well. These features were not magnetospheric in ori-
 180 gin, as the P1 electron PAD during this time was isotropic and featureless.

181 To determine whether each probe was connected to the Moon, we calculate the “im-
 182 pact parameter” (Van Allen & Ness, 1969): we project a line parallel to the observed mag-
 183 netic field vector toward the lunar surface at each point. If this line intersects the sur-
 184 face, this parameter is $\leq 1R_L$ and the probe was connected to a field line that threaded
 185 the lunar disk. The times when this occurred are indicated by black horizontal bars in
 186 panel 2e. This approximation cannot account for changes in the magnetic field that oc-
 187 cur *between* the probe and the Moon (e.g., crustal anomalies), but is estimated to be ac-
 188 curate to within 2° ($\sim 0.07R_L$ for each $2R_L$ in altitude; see Van Allen & Ness, 1969;
 189 Van Allen, 1970). The shadows in the SEE flux across multiple pitch angles and ener-
 190 gies closely coincide with times when the probes were magnetically connected to the lu-
 191 nar surface, showing a correlation between the probes’ magnetic connection and the re-
 192 duced SEE fluxes. This is especially visible for P1 which was only disconnected from the
 193 surface near 19:30 UTC, coinciding with a brief region where the 1–10keV PAD showed
 194 no clear depletion, although there are larger deviations for P2 which are discussed be-
 195 low.

196 To further investigate the relationship between magnetic connectedness and the ob-
 197 served solar energetic electron shadows, Figure 2f displays a simplified schematic of the
 198 lunar environment in the GSE x - y plane, along with the ARTEMIS probes’ trajectories,
 199 during the 31 July 2023 SEE event. The magnetospheric field was predominantly point-
 200 ing down-tail (see panel 2e) and the perpendicular bulk plasma velocity was ~ 20 km/s,
 201 with components along the $-y$ and $-z$ axes; i.e., the magnetotail was convecting south-
 202 ward and along the Moon’s orbital direction (see Figure S2 in the Supporting Informa-
 203 tion).

204 Assuming the SEEs during the 31 July 2023 event entered Earth’s magnetotail from
 205 far downstream, electrons approaching the Moon from down-tail and located within the
 206 region defined by $\sqrt{y^2 + z^2} \leq R_L$ would impact the nightside lunar surface (gray half-
 207 circle in Figure 2f). An Earthward-traveling electron located just outside of this cylin-
 208 der near the dusk terminator (with pitch angle $\alpha = 180^\circ$) would just pass the lunar sur-

face without impacting (green arrow labeled “Final Earthward SEE” in panel 2f). Ignoring pitch angle scattering, this electron would mirror near the Earth and travel back toward the Moon with a pitch angle of $\alpha = 0^\circ$ (green “Final reflected SEE”). In the finite time required for the electron to travel the $\sim 120R_E$ round-trip, the magnetic field line along which the electron is bouncing has convected a distance Δy along the $-y$ axis, and this electron would impact the dayside lunar surface. The width Δy of this region is energy-dependent, ranging from $0.35\text{--}0.03R_L$ for electrons with initially aligned pitch angles that mirror at Earth with energies between $1 \text{ keV} \leq E \leq 300 \text{ keV}$. In cis-lunar space, this process therefore generates a void in the distribution of *Earthward*-traveling electrons (red shading in panel 2f; see also Van Allen, 1970).

Similarly, we can consider an Earthward-traveling electron initially down-tail of the Moon and near the dawn terminator that lies just outside the region defined by $\sqrt{y^2 + z^2} \leq R_L$. This electron would travel past the Moon without impacting the lunar surface (labeled “First Earthward SEE” in orange), reflect near Earth, and return to the Moon. Again, the convection of the magnetotail causes a displacement of Δy for this electron along the Moon’s orbital direction, generating a shadow of *reflected* electrons (blue shading in panel 2f). Between these two regions, *no* SEEs are present in cis-lunar space: Earthward-traveling electrons would have impacted the lunar nightside surface, so a drop-out in electrons forms at all pitch angles.

Panel 2f shows that for this simplified scenario, P1 would first encounter a shadow of Earthward-traveling ($90^\circ < \alpha \leq 180^\circ$) electrons near 18:00 UTC, followed by a drop-out at all pitch angles, and finally a shadow in reflected SEEs ($0^\circ \leq \alpha < 90^\circ$) after passing into the nightside. For P2, Figure 2f suggests the reverse order since its orbit direction is counter-clockwise compared to the clockwise orbit of P1: first, P2 would detect a shadow of reflected electrons, then across all pitch angles, followed by a drop-out for the Earthward-traveling electrons.

Figures 2a–2d show that the ARTEMIS observations of electron shadows are consistent with this behavior. P1 was connected to the lunar surface for approximately 1.5 h beginning near 18:30 UTC, where ESA observed a reduction in the differential electron flux (the SST attenuator was engaged so higher-energy electrons were not measured). The pitch angle distribution of these electrons is consistent with the shadow behavior illustrated in Figure 2f: an initial drop-out in the Earthward-traveling electrons ($90^\circ <$

$\alpha \leq 180^\circ$) was observed, followed by a reduced flux at all pitch angles from 18:42 UTC through 19:20 UTC, when the probe crossed into the lunar nightside. After this point, the probe encountered a reflected electron shadow, characterized by reduced fluxes of $0^\circ \leq \alpha < 90^\circ$ electrons until approximately 19:50 UTC. The electron flux was briefly filled in near 19:30 UTC, coinciding with the time that P1's magnetic connection to the surface was temporarily disrupted as the probe crossed the lunar terminator.

Using the observed shadows, we can estimate the convection velocity of the tail. The shadow of Earthward-traveling, 1–10 keV electrons initially detected by P1 between 18:30 UTC and 18:42 UTC had a width of $\Delta y = 0.39R_L$ along P1's orbit. The time for a field-aligned, 1 keV electron to travel from the Moon to its mirror point at Earth ($60R_E$ away) and back is 41 s, while a 10 keV electron completes this round-trip in 13 s. These values, along with the observed width of the shadow, suggest that the tail convection velocity was between 16–50 km/s along the y -direction, which is consistent with the ARTEMIS observations of the cold, $\mathbf{E} \times \mathbf{B}$ drifting ion population at this time (see Figure S2 of the Supporting Information).

For P2, the probe was estimated to be magnetically connected to the lunar surface beginning near 15:10 UTC, where it detected a shadow in the reflected electron population (pitch angles $0^\circ \leq \alpha < 90^\circ$) that was sustained for ~ 30 min. This drop-out was initially detected in the ESA for 1–10 keV electrons, before extending to the SST instrument at energies 40–100 keV. Near 15:30 UTC, a drop-out at all pitch angles was observed for ~ 5 min at energies $1 \text{ keV} \leq E \leq 300 \text{ keV}$, after which the probe again passed through a reflected electron shadow. Similar features, alternating between reflected and full electron shadows, were observed by P2 until approximately 17:00 UTC. Finally, near 19:30 UTC, P2 again detected a drop-out across all electron pitch angles, followed by a brief detection of a reflected electron shadow.

Despite the promising agreement between the schematic in Figure 2f and the electron PADs observed by P1, there are deviations from this simplified picture for P2. Although the impact parameter calculation suggests that P2 was connected to the surface continuously from 15:00–17:30 UTC, the probe did not detect a single shadow during this time. Instead, P2 measured distinct intervals of shadowing that were separated by up to 30 min. In addition, the first observed shadow was seen approximately 2.5 h earlier than Figure 2f suggests. These discrepancies are likely caused by changes in the mag-

273 netic field vector between the spacecraft and surface and non-uniform magnetotail con-
 274 vection patterns during this time (including convection out of the plane displayed in Fig-
 275 ure 2f), which caused this magnetic connection to be severed. Besides, since P2 was lo-
 276 cated $\sim 10R_L$ from the Moon, there are large uncertainties (up to $0.35R_L$) in the im-
 277 pact parameter calculation. Regardless, Figure 2 shows evidence for SEE shadowing by
 278 the lunar surface that are sustained through extended regions of the magnetotail.

279 3.2 Modeling SEE access to the lunar surface

280 To determine locations across the lunar surface that are accessible to initially Earthward-
 281 traveling SEEs, we modeled the precipitation patterns of these electrons using the rel-
 282 ativistic GENTOO model (Liuzzo et al., 2019a), which has been applied for studies of
 283 multiple moons throughout the solar system (e.g., Addison et al., 2021, 2022; Breer et
 284 al., 2019; Liuzzo et al., 2019b, 2020; Liuzzo, Poppe, Addison, et al., 2022; Liuzzo, Poppe,
 285 et al., 2024; Liuzzo, Nénon, et al., 2024). For select energies, electrons were initialized
 286 at a given a velocity (determined by the particle's energy), pitch angle (with a resolu-
 287 tion of 2°), and gyrophase (with a 4° resolution), and their dynamics are modeled while
 288 they remain within a distance of $\sim 10R_L$ from the lunar surface; i.e., we do not con-
 289 sider electrons that are mirrored near Earth. We aligned the magnetic field with the GSE
 290 $-x$ axis with a magnitude of $|\mathbf{B}| = 10$ nT and assumed no perpendicular convection,
 291 consistent with typical magnetotail lobe conditions (see Liuzzo, Poppe, & Halekas, 2022;
 292 Runov et al., 2023).

293 Figures 3a–3d display the percentages of Earthward-traveling SEEs that precip-
 294 itate onto a given location on the lunar surface for select energies ranging from $100 \text{ keV} \leq$
 295 $E \leq 100 \text{ MeV}$. Although this upper limit extends beyond the energy range detectable
 296 by ARTEMIS and Wind, it allows us to investigate precipitation patterns for electrons
 297 whose gyroradii exceed the size of the Moon. Figure 3e shows this percentage along the
 298 equator for various electron energies, while Figure 3f illustrates the relativistic electron
 299 gyroradii as a function of pitch angle. As visible in panel 3a, nearly all the 0.1 MeV elec-
 300 trons (gyroradii $r_g \leq 0.06R_L$) precipitate onto the nightside (trans-lunar) surface. To
 301 illustrate this further, the white dashed line in panel 3a denotes the contour where only
 302 10% of electrons reach the surface. Since their gyroradii are small compared to the size
 303 of the Moon, only few 0.1 MeV electrons that originate from down-tail precipitate onto
 304 the dayside and this contour is nearly co-located with the terminators (marked “dusk”

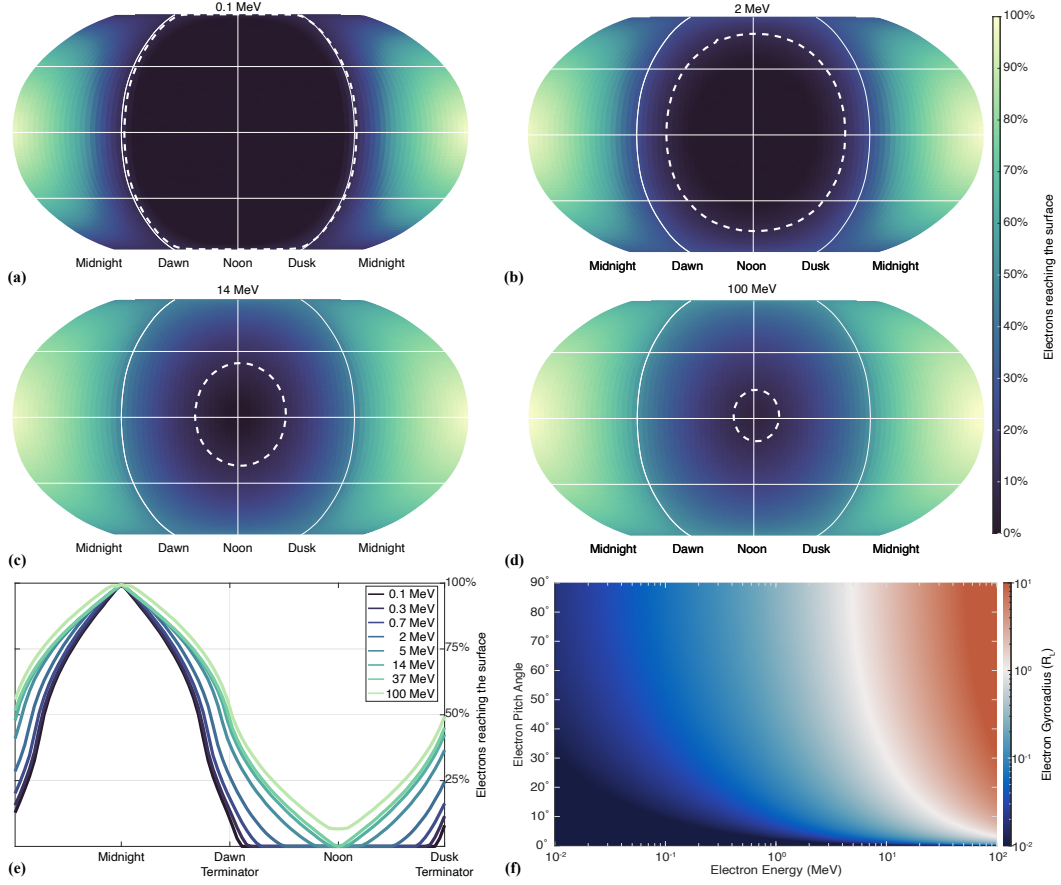


Figure 3. Relativistic electron (a–d) precipitation maps with the 10% contour given by the dashed-white line, (e) equatorial access at select energies, and (f) pitch angle and gyroradii.

and “dawn”). This nightside precipitation forms the electron shadows in cis-lunar space, as detected by ARTEMIS when magnetically connected to the Moon (see Figure 2).

The precipitation patterns are qualitatively similar across multiple energies (see panels 3b–3d), with access of Earthward-traveling SEEs gradually expanding into the cis-lunar hemisphere with increasing energy. The growing gyroradii allows an increasing fraction of electrons near perpendicular pitch angles to reach beyond the terminator and the 10% accessibility contours approach the subsolar point. However, even with gyroradii that eventually exceed the radius of the Moon by an order of magnitude for the highest energy studied here, Earthward-traveling SEEs still do not uniformly irradiate the surface, with only $\sim 10\%$ of 100 MeV electrons reaching the subsolar point (which here coincides with the region where the magnetic field vector is normal to the

³¹⁶ Moon's surface). Indeed, the access of SEEs to the equatorial lunar dayside drops pre-
³¹⁷ cipitously when crossing the terminators, regardless of particle energy (panel 3e).

³¹⁸ There are several caveats associated with interpretation of Figure 3. For example,
³¹⁹ we assume the ambient magnetic field is uniform and oriented in the $-x$ -direction (anti-
³²⁰ Sunward), which is representative of the local magnetospheric field within the magne-
³²¹ totail lobes (Liuzzo et al., 2021; Liuzzo, Poppe, & Halekas, 2022) but does not hold true
³²² over scales of multiple R_E , and we have ignored perpendicular drifts over similar length
³²³ scales. Changes to the electrons' trajectories associated with these effects are not rep-
³²⁴ resented in this approach, and we caution that these results should *not* be interpreted
³²⁵ as a complete lack of electron precipitation across the dayside surface. However, these
³²⁶ results are consistent with observations of electron shadows in cis-lunar space that re-
³²⁷ duce precipitation of SEEs onto the dayside when the Moon is in the tail as shown in
³²⁸ Figures 1 and 2.

³²⁹ 4 Discussion and Conclusions

³³⁰ We have focused on two case-studies to show that solar energetic electrons access
³³¹ the lunar environment even when embedded within the terrestrial magnetotail. For two
³³² separate SEE events, we find that the tail is open to these particles with fluxes that were
³³³ nearly unaltered compared to their distribution upstream and show that they have di-
³³⁴ rect access to the lunar nightside surface. Finally, we have identified electron shadows
³³⁵ that extend through cis-lunar space, where structured and sustained drop-outs in the
³³⁶ flux of Earthward-traveling and (reflected) tailward-traveling SEEs span multiple orders
³³⁷ of magnitude in energy. Importantly, while our findings suggest that the lunar dayside
³³⁸ surface flux is relatively reduced compared to the flux onto the nightside during SEE events,
³³⁹ these results indicate that high-energy electrons during solar particle events have direct
³⁴⁰ access to the lunar orbit within the magnetotail. A detailed comparison between the tem-
³⁴¹ poral dispersion in the SEE arrival times at Wind and ARTEMIS across a range of en-
³⁴² ergies would allow for a greater understanding of where these electrons gain access to
³⁴³ the magnetotail, but this is not possible for these events due to the instruments' sam-
³⁴⁴ ple rates.

³⁴⁵ Multiple identifications of these electron shadows by ARTEMIS indicate they are
³⁴⁶ common features during solar energetic electron events; a table and additional observa-

tions are provided in the Supporting Information. Electron shadows were also seen by Explorer 35, with Lin (1968) and Van Allen and Ness (1969) suggesting that they preferentially occur in cis-lunar space within a few radii of the Moon's surface when in the magnetotail. However, we have shown that shadows in Earthward-traveling electrons extend far from the surface and are clearly identifiable in particle data taken at least $\sim 10R_L$ from the Moon. In addition, we have illustrated that Earthward-traveling SEEs can pass the Moon, be reflected in the enhanced field near Earth, and precipitate onto the lunar dayside. Not only does this behavior tend to isotropize the SEE population within the magnetotail, but it generates an additional electron shadow in trans-lunar space. The reduced flux of this reflected (tailward-traveling) population suggests that the shadows must persist at distances $\gg 10R_L$ from the Moon. Hence, we propose that the only requirement for future detections of these shadows is a magnetic connection to the lunar surface during a SEE event, with some portion of the population counter-streaming across the opposite side of the Moon. There is therefore no stipulation for isotropy (or lack thereof) of the incident electron population to generate these shadows in the particle distribution (cf. Anderson & Lin, 1969; Van Allen, 1970). These results are important for the fundamental scientific understanding of SEEs and their access to the lunar surface. In addition, our findings have important implications in the context of exploration of the near-lunar environment by the upcoming crewed Artemis and Lunar Gateway missions.

366 Open Research

367 THEMIS-ARTEMIS data are available at sprg.ssl.berkeley.edu/data/themis and Wind
 368 data can be accessed at sprg.ssl.berkeley.edu/data/wind. Analysis software for ARTEMIS
 369 is available through the Space Physics Environment Data Analysis Software (Angelopoulos
 370 et al., 2019) and analysis software for Wind can be found at Wilson (2021).

371 Acknowledgments

372 The authors are supported by NASA Lunar Data Analysis Program grant 80NSSC23K1338.
 373 L.L. thanks L.B. Wilson III for insight into Wind 3DP. The authors acknowledge NASA
 374 contract NAS5-02099 for the use of ARTEMIS data, and specifically, J.P. McFadden for
 375 use of ESA data and K.-H. Glassmeier, U. Auster, and W. Baumjohann for the use of
 376 FGM data provided under the lead of the Technical University of Braunschweig with fi-

377 nancial support through the German Ministry for Economy and Technology and the Ger-
 378 man Center for Aviation and Space, Contract 50-OC-0302.

379 **References**

- 380 Addison, P., Liuzzo, L., Arnold, H., & Simon, S. (2021, 5). Influence of Europa's
 381 Time-Varying Electromagnetic Environment on Magnetospheric Ion Precipita-
 382 tion and Surface Weathering. *Journal of Geophysical Research: Space Physics*,
 383 *126*(5), 1–42. doi: 10.1029/2020JA029087
- 384 Addison, P., Liuzzo, L., & Simon, S. (2022, 2). Effect of the Magnetospheric Plasma
 385 Interaction and Solar Illumination on Ion Sputtering of Europa's Surface
 386 Ice. *Journal of Geophysical Research: Space Physics*, *127*(2), 1–39. doi:
 387 10.1029/2021JA030136
- 388 Anderson, K. A., & Lin, R. P. (1969, 8). Observation of interplanetary field lines in
 389 the magnetotail. *Journal of Geophysical Research*, *74*(16), 3953–3968. doi: 10
 390 .1029/JA074i016p03953
- 391 Angelopoulos, V. (2011, 12). The ARTEMIS Mission. *Space Science Reviews*, *165*(1–
 392 4), 3–25. doi: 10.1007/s11214-010-9687-2
- 393 Angelopoulos, V., Cruce, P., Drozdov, A., Grimes, E. W., Hatzigeorgiu, N., King,
 394 D. A., ... Schroeder, P. (2019). *The Space Physics Environment Data
 395 Analysis System (SPEDAS)* (Vol. 215) (No. 1). The Author(s). doi:
 396 10.1007/s11214-018-0576-4
- 397 Breer, B. R., Liuzzo, L., Arnold, H., Andersson, P. N., & Simon, S. (2019, 9). Ener-
 398 getic ion dynamics in the perturbed electromagnetic fields near Europa. *Jour-
 399 nal of Geophysical Research: Space Physics*, *124*(9), 7592–7613. doi: 10.1029/
 400 2019JA027147
- 401 Harten, R., & Clark, K. (1995). The design features of the GGS wind and polar
 402 spacecraft. *Space Science Reviews*, *71*(1–4), 23–40. doi: 10.1007/BF00751324
- 403 Jordan, A. P., Wilson, J. K., & Spence, H. E. (2023, 2). Energetic charged particle
 404 dose rates in water ice on the Moon. *Icarus*, *115477*. doi: 10.1016/j.icarus.2023
 405 .115477
- 406 Lin, R. P. (1968, 5). Observations of lunar shadowing of energetic particles. *Journal
 407 of Geophysical Research*, *73*(9), 3066–3071. doi: 10.1029/JA073i009p03066
- 408 Lin, R. P., Anderson, K. A., Ashford, S., Carlson, C., Curtis, D., Ergun, R., ...

- 409 Paschmann, G. (1995, 2). A three-dimensional plasma and energetic parti-
410 cle investigation for the Wind spacecraft. *Space Science Reviews*, 71(1-4),
411 125–153. doi: 10.1007/BF00751328
- 412 Liuzzo, L., Nénon, Q., Poppe, A. R., Stahl, A., Simon, S., & Fatemi, S. (2024). On
413 the formation of trapped electron radiation belts at Ganymede. *Geophysical*
414 *Research Letters*, 51. doi: 10.1029/2024GL109058
- 415 Liuzzo, L., Poppe, A. R., Addison, P., Simon, S., Nénon, Q., & Paranicas, C.
416 (2022, 11). Energetic Magnetospheric Particle Fluxes Onto Callisto’s At-
417 mosphere. *Journal of Geophysical Research: Space Physics*, 127(11), 1–30. doi:
418 10.1029/2022JA030915
- 419 Liuzzo, L., Poppe, A. R., & Halekas, J. S. (2022). A Statistical Study of the Moon’s
420 Magnetotail Plasma Environment. *Journal of Geophysical Research: Space*
421 *Physics*, 127(4), 1–23. doi: 10.1029/2022JA030260
- 422 Liuzzo, L., Poppe, A. R., Halekas, J. S., Simon, S., & Cao, X. (2021, 5). Investi-
423 gating the Moon’s Interaction With the Terrestrial Magnetotail Lobe Plasma.
424 *Geophysical Research Letters*, 48(9), 1–11. doi: 10.1029/2021GL093566
- 425 Liuzzo, L., Poppe, A. R., Lee, C. O., Xu, S., & Angelopoulos, V. (2023, 6). Un-
426 restricted Solar Energetic Particle Access to the Moon While Within the
427 Terrestrial Magnetotail. *Geophysical Research Letters*, 50(12), 1–9. doi:
428 10.1029/2023GL103990
- 429 Liuzzo, L., Poppe, A. R., Nénon, Q., Simon, S., & Addison, P. (2024). Constraining
430 the Influence of Callisto’s Perturbed Electromagnetic Environment on Ener-
431 getic Particle Observations. *Journal of Geophysical Research: Space Physics*.
432 doi: 10.1029/2023JA032189
- 433 Liuzzo, L., Poppe, A. R., Paranicas, C., Nénon, Q., Fatemi, S., & Simon, S. (2020,
434 9). Variability in the energetic electron bombardment of Ganymede. *Journal of*
435 *Geophysical Research: Space Physics*, 1–35. doi: 10.1029/2020JA028347
- 436 Liuzzo, L., Simon, S., & Regoli, L. (2019a, 12). Energetic electron dynamics near
437 Callisto. *Planetary and Space Science*, 179(August), 104726. doi: 10.1016/j.pss
438 .2019.104726
- 439 Liuzzo, L., Simon, S., & Regoli, L. (2019b, 2). Energetic ion dynamics near Callisto.
440 *Planetary and Space Science*, 166, 23–53. doi: 10.1016/j.pss.2018.07.014
- 441 McFadden, J. P., Carlson, C. W., Larson, D., Ludlam, M., Abiad, R., Elliott,

- 442 B., ... Angelopoulos, V. (2008). The THEMIS ESA plasma instrument
443 and in-flight calibration. *Space Science Reviews*, 141(1-4), 277–302. doi:
444 10.1007/s11214-008-9440-2
- 445 Runov, A., Angelopoulos, V., Khurana, K., Liu, J., Balikhin, M., & Artemyev,
446 A. V. (2023). Properties of Quiet Magnetotail Plasma Sheet at Lunar
447 Distances. *Journal of Geophysical Research: Space Physics*, 128(11). doi:
448 10.1029/2023JA031908
- 449 Terada, K., Yokota, S., Saito, Y., Kitamura, N., Asamura, K., & Nishino, M. N.
450 (2017, 1). Biogenic oxygen from Earth transported to the Moon by
451 a wind of magnetospheric ions. *Nature Astronomy*, 1(2), 0026. doi:
452 10.1038/s41550-016-0026
- 453 Van Allen, J. A. (1970). Energetic Particle Phenomena in the Earth's Magneto-
454 spheric Tail. In B. M. McCormac (Ed.), *Particles and fields in the magneto-*
455 *sphere* (Vol. 17, pp. 111–121). Dordrecht: Springer Netherlands. doi: 10.1007/
456 978-94-010-3284-1
- 457 Van Allen, J. A., & Ness, N. F. (1969, 1). Particle shadowing by the Moon. *Journal*
458 *of Geophysical Research*, 74(1), 71–93. doi: 10.1029/JA074i001p00071
- 459 Wilson, L. B. (2021). *lynnbwilsoniii/wind_3dp_pros: Space Plasma Missions IDL*
460 *Software Library*. [Software]. Zenodo. doi: 10.5281/zenodo.4451330